

Strongly correlated metal interfaces in the Gutzwiller approximation

Giovanni Borghi,¹ Michele Fabrizio,^{1,2} and Erio Tosatti^{1,2}

¹*International School for Advanced Studies (SISSA),*

and CRS Democritos, CNR-INFM, Via Beirut 2-4, I-34151 Trieste, Italy

²*The Abdus Salam International Centre for Theoretical Physics (ICTP), P.O.Box 586, I-34151 Trieste, Italy*

We study the effect of spatial inhomogeneity on the physics of a strongly correlated electron system exhibiting a metallic phase and a Mott insulating phase, represented by the simple Hubbard model. In three dimensions, we consider various geometries, including vacuum-metal-vacuum, a junction between a weakly and a strongly correlated metal, and finally the double junctions metal-Mott insulator-metal and metal-strongly correlated metal-metal. We applied to these problems the self-consistent Gutzwiller technique recently developed in our group, whose approximate nature is compensated by an extreme flexibility, ability to treat very large systems, and physical transparency. The main general result is a clear characterization of the position dependent metallic quasiparticle spectral weight. Its behavior at interfaces reveals the ubiquitous presence of exponential decays and crossovers, with decay lengths of clear physical significance. The decay length of metallic strength in a weakly-strongly correlated metal interface is due to poor screening in the strongly correlated side. The decay length of metallic strength from a metal into a Mott insulator (or into vacuum) is due to tunneling. In both cases, the decay length is a bulk property, and diverges with a critical exponent ($\sim 1/2$ in the present approximation, mean field in character) as the (continuous, paramagnetic) Mott transition is approached.

I. INTRODUCTION

Metallic electron wavefunction delocalization in a lattice of atoms or molecules is caused by the lowering of electron kinetic energy and by the simultaneous improvement of electron-ion Coulomb attraction. By abandoning the ion cores and turning delocalized, an electron can in fact feel the potential of more than one nucleus. However, coherent electron motion is opposed by the mutual electron-electron Coulomb repulsion, which is higher when electrons move due to their higher chance of colliding when visiting the same site. When the first two terms prevail, the system is a conventional band insulator or metal, depending whether the Fermi level falls in a band gap or across one or more bands. When the electron-electron repulsion prevails instead the electrons localize on their atomic or molecular sites leading to a so-called Mott insulator¹. Despite that conceptual simplicity, properties of Mott insulators and especially of strongly correlated metals in the proximity of a Mott metal-insulator transition as a function of increasing correlations remain quite difficult to capture both theoretically and experimentally. Theoretically, the reason is that the Mott transition is a collective phenomenon, which escapes single-particle or mean field theories such as Hartree-Fock or density-functional-theory within the local-density approximation (LDA). Experimentally, additional complications such as magnetism, lattice distortions, etc., often conspire to mask the real nature of the Mott localization phenomenon.

Important insights into this problem have been gained in the last two decades especially thanks to dynamical mean field theory (DMFT).² DMFT predicts that, as the electron-electron repulsion – usually parametrized by a short-range Hubbard repulsion U – increases, the ordinary band metal evolves first to a *strongly correlated*

metal well before the Mott transition. In the strongly correlated metal the electron spectral function undergoes a profound change, exhibiting well formed Mott-Hubbard side-bands coexisting with delocalized quasiparticles, the latter narrowly centered in energy near the Fermi level. Only successively upon increasing repulsion do the quasiparticles disappear as the Mott transition takes place at $U = U_{\text{crit}}$. This intriguing prediction – simultaneous metallic and insulating features, exhibited on well separated energy scales – has stimulated a considerable experimental effort to reveal coexisting quasiparticles and Mott-Hubbard bands in strongly correlated metals^{3,4,5,6,7,8,9,10,11,12}, especially in the paradigmatic system V_2O_3 . This is the compound where a Mott transition has been first discovered¹³ and theoretically studied^{14,15}. At ambient temperature and pressure V_2O_3 is a correlated metal. It undergoes a first-order Mott transition at $\sim T_N \simeq 155$ K to an antiferromagnetic insulator accompanied by a monoclinic distortion of the high temperature corundum structure.¹⁶ The paramagnetic high-temperature metal can moreover be turned into a paramagnetic Mott insulator upon substituting V with bulkier Cr, $(\text{V}_{1-x}\text{Cr}_x)_2\text{O}_3$. For $0.005 < x < 0.017$ a first-order line separates the high temperature metal from the paramagnetic Mott insulator, which terminates with a critical point at $T \simeq 400$ K and $x \simeq 0.005$.

Near the metal-insulator transition of $(\text{V}_{1-x}\text{Cr}_x)_2\text{O}_3$, the strongly correlated metal must of course possess well defined quasiparticles at the Fermi energy. Surprisingly, early photoemission experiments^{17,18,19,20} failed to reveal the sharp quasiparticle peak predicted by DMFT at E_F . The electronic spectrum appeared instead dominated by the lower Mott-Hubbard band with barely a hint of metallic weight at the Fermi energy. It was recognized only later that photoemission in strongly correlated metals is highly surface-sensitive.^{3,4,6,7,11,12,21} By

increasing the photon frequency, which corresponds to more energetic excited photo-electrons, i.e. longer escape lengths, a prominent quasiparticle peak coexisting with incoherent Mott-Hubbard bands was eventually observed in V_2O_3 ^{5,10,22}. Quasiparticle suppression in surface-sensitive probes was attributed²² to surface-modified Hamiltonian parameters, the reduced atomic coordination pushing the surface closer to the Mott transition than the underlying bulk. This conclusion, although not unreasonable, raises however a more fundamental question. A metal does not possess any intrinsic long-distance electronic length-scale other than the Fermi wavelength. Thus an imperfection like a surface can only induce a power-law decaying disturbance such as that associated with Friedel's oscillations. Since one does not expect Luttinger's theorem to break down, these oscillations should be controlled by the same Fermi wavelength as in the absence of interaction, irrespectively of the proximity of the Mott transition. On the other hand, a strongly correlated metal does possess an intrinsic energy scale, the parametric distance of the Hamiltonian from the Mott transition, and that could be associated with a length scale. For example, the arising of a critical length scale in association with a free energy scale is well known in second order phase transitions. The surface as a perturbation may alter the quasiparticle properties within a depth corresponding to that characteristic length. We expect this length to be a bulk property, the longer the closer the Mott transition, unlike the Fermi wavelength that remains constant. In this respect, it is not *a priori* clear whether the recovery of bulk-quasiparticle spectral properties with increasing depth should be power-law, compatible with the common view of a metal as an inherently critical state of matter, or exponential, as one would expect by regarding the Mott transition as any other critical phenomena where power laws emerge only at criticality.

Besides the interface with vacuum, which is relevant to spectroscopy, other types of interface involving correlated materials are attracting increasing interest. In 2004, Ohtomo and Hwang²³ discovered that the interface between two insulating oxides, $LaAlO_3$ and $SrTiO_3$, is a high-mobility two-dimensional conductor that even shows superconductivity²⁴. This discovery stimulated experimental and theoretical studies on oxides heterostructures²⁵. On the theory side, some activity has been focused either on the characterization of the electronic structure of these interfaces by *ab-initio* LDA calculations, see e.g. Ref. 26, as well as on DMFT analyses of simple models^{27,28,29,30,31,32,33,34,35} and on combined LDA-DMFT calculations³⁶ aimed at understanding interface correlation effects poorly described within straight LDA. The DMFT approaches adopted in the literature to describe this kind of situations were *ad-hoc* extensions of the single-site DMFT² to inhomogeneous systems.^{27,28} In the specific example of a layered structure, the electron self-energy was assumed to depend, besides the frequency, also upon the layer index. In this scheme

the self-energy is calculated by solving an auxiliary impurity model for each layer in which the conducting bath depends self-consistently on the fully-interacting impurity Green's functions not only of that given layer but also of the nearby ones. This additional complication with respect to conventional DMFT weighs on the numerical calculation, which is thus limited to few tens of layers. Although this is adequate for the interface between two insulators, such as that studied by Ohtomo and Hwang²³, it is generally insufficient in other cases, such as the surface effects in the interior of a correlated metal,³⁷ or any other interface involving at least one metal.

Recently, we proposed an alternative theoretical approach to interface problems,³⁸ based on the extension of the Gutzwiller wavefunction and approximation^{39,40} to inhomogeneous situations. The method, although a further approximation beyond DMFT, hence in principle less accurate, is much more agile, and can treat without effort hundreds of layers. Thus it can be used as a complementary tool to extrapolate DMFT results to large sizes, otherwise inaccessible by straight DMFT.

In this work, we shall extend the analysis of Ref. 38 for the vacuum/correlated-metal interface to other model interfaces that might be relevant for experiments: the junction between two different correlated metals and the tunneling between two metallic leads through a strongly correlated, possibly Mott insulating, region. Although both cases were in fact previously studied by DMFT^{31,34,35}, the results were interpreted in contrasting ways. While Helmes *et al.*³⁴ concluded that the Mott insulator is impenetrable to the electrons coming from the metallic leads, Zenia *et al.*³⁵ drew the opposite conclusion that a conducting channel always open up inside the insulator at sufficiently low temperature. The present study, which is certainly less accurate than DMFT but can deal with much larger sizes, will also serve to clarify this issue. In particular, the large sizes allow us to address the asymptotic behavior and to identify the magnitude and interface role of the critical length associated with the bulk Mott transition.

The paper is organized as follows. In section II we introduce the model Hamiltonian, which is a Hubbard model with layer dependent parameters, and a Gutzwiller variational scheme adapted for such an inhomogeneous situation. We then study in section III three different slab geometries: (a) strong correlated metal-vacuum interface; (b) junction between two different correlated metals; (c) a Mott insulator or a strongly correlated metal sandwiched between two weakly correlated metals. In the first two cases we find that the perturbation induced by the surface inside the bulk of the correlated metal decay exponentially at long distances. The length scale ξ that controls this decay is a bulk property that depends in our simplified model only on $U_{\text{crit}} - U$ and diverges on approaching the Mott transition like $\xi \sim (U_{\text{crit}} - U)^{-\nu}$, with a mean-field like exponent $\nu \simeq 0.5$. The last case (c) is more interesting. Either when the central region, of width d , is a strongly correlated metal, $U_{\text{center}} < U_{\text{crit}}$

or when it is a Mott insulator, $U_{\text{center}} > U_{\text{crit}}$, the effects of the two metal leads are found to decay exponentially over a length ξ . Just like in cases (a) and (b) above, ξ is only controlled by the distance from Mott criticality, i.e.

$$\xi \sim |U_{\text{crit}} - U_{\text{center}}|^{-0.5},$$

which therefore appears naturally as a correlation length that is finite on both sides of the transition. However, while the quasiparticle weight saturates to a finite constant determined by $U_{\text{center}} < U_{\text{crit}}$ and independent of d when the central region is a strongly correlated metal, in the opposite case of a Mott insulator the quasiparticle weight saturates to a finite value exponentially small in d . Interestingly, right at criticality, $U_{\text{center}} = U_{\text{crit}}$, the saturation value decays power law in d . Finally, section IV is devoted to concluding remarks. For a better understanding of our numerical data, a simple analytical model for the spatial dependence of quasiparticle weight is set up in appendix A, while in appendix B we discuss the effects of electron-electron interaction on the physics of Friedel's oscillations near surfaces and junctions within the Gutzwiller approximation.

II. MODEL AND METHOD

In order to address the generic interface features of a strongly correlated metal, we consider the simplest Hamiltonian exhibiting a Mott transition, namely the Hubbard model

$$H = - \sum_{\langle \mathbf{R}\mathbf{R}' \rangle_{\sigma}} t_{\mathbf{R}\mathbf{R}'} (c_{\mathbf{R}\sigma}^{\dagger} c_{\mathbf{R}'\sigma} + H.c.) + \sum_{\mathbf{R}} \epsilon_{\mathbf{R}} n_{\mathbf{R}} + U_{\mathbf{R}} n_{\mathbf{R}\uparrow} n_{\mathbf{R}\downarrow}, \quad (1)$$

where $\langle \mathbf{R}\mathbf{R}' \rangle$ denotes nearest neighbor sites, $c_{\mathbf{R}\sigma}^{\dagger}$ and $c_{\mathbf{R}\sigma}$ creates and annihilates, respectively, an electron at site \mathbf{R} with spin σ , and finally $n_{\mathbf{R}\sigma} = c_{\mathbf{R}\sigma}^{\dagger} c_{\mathbf{R}\sigma}$ and $n_{\mathbf{R}} = n_{\mathbf{R}\uparrow} + n_{\mathbf{R}\downarrow}$. In our inhomogeneous system, all Hamiltonian parameters are allowed to be site dependent. For interfaces, we shall assume an N -layer slab geometry where all parameters are constant within each layer, identified by a layer coordinate $z = 1, \dots, N$ but generally different from layer to layer. For instance, the hopping between nearest neighbor sites \mathbf{R} and \mathbf{R}' within layer z depends only on z , i.e. $t_{\mathbf{R}\mathbf{R}'} = t(z)$, while if \mathbf{R} and \mathbf{R}' belong to nearby layers, e.g. z and $z \pm 1$, then $t_{\mathbf{R}\mathbf{R}'} = t(z, z \pm 1) = t(z \pm 1, z)$.

We study the Hubbard Hamiltonian (1) in the non-magnetic (also called paramagnetic) sector by means of a Gutzwiller type variational wavefunction

$$|\Psi\rangle = \prod_{\mathbf{R}} \mathcal{P}_{\mathbf{R}} |\Psi_0\rangle, \quad (2)$$

where $|\Psi_0\rangle$ is a paramagnetic Slater determinant. Because of our choice of layer-dependent parameters, the

operator $\mathcal{P}_{\mathbf{R}}$ has the general expression

$$\mathcal{P}_{\mathbf{R}} = \sum_{n=0}^2 \lambda_n(z) |n, \mathbf{R}\rangle \langle n, \mathbf{R}|, \quad (3)$$

where $|n, \mathbf{R}\rangle \langle n, \mathbf{R}|$ is the projector at site $\mathbf{R} = (x, y, z)$, (x and y are intralayer coordinates), onto configurations with n electrons (note that $|1, \mathbf{R}\rangle \langle 1, \mathbf{R}| \equiv \sum_{\sigma} c_{\mathbf{R}\sigma}^{\dagger} |0, \mathbf{R}\rangle \langle 0, \mathbf{R}| c_{\mathbf{R}\sigma}$), and $\lambda_n(z)$ are layer-dependent variational parameters. We calculate quantum averages on $|\Psi\rangle$ using the so-called Gutzwiller approximation^{39,40}, (for details see e.g. Ref.⁴¹ whose notations we use hereafter) and require that

$$\langle \Psi_0 | \mathcal{P}_{\mathbf{R}}^2 | \Psi_0 \rangle = 1, \quad (4)$$

$$\langle \Psi_0 | \mathcal{P}_{\mathbf{R}}^2 n_{\mathbf{R}\sigma} | \Psi_0 \rangle = \langle \Psi_0 | n_{\mathbf{R}\sigma} | \Psi_0 \rangle \equiv \frac{n(z)}{2}. \quad (5)$$

Explicitly, these two conditions imply that

$$1 = \left(1 - \frac{n(z)}{2}\right)^2 \lambda_0(z)^2 + n(z) \left(1 - \frac{n(z)}{2}\right) \lambda_1(z)^2 + \frac{n(z)^2}{4} \lambda_2(z)^2, \quad (6)$$

$$n(z) = n(z) \left(1 - \frac{n(z)}{2}\right) \lambda_1(z)^2 + 2 \frac{n(z)^2}{4} \lambda_2(z)^2. \quad (7)$$

We note that $n(z)$ is fixed once the uncorrelated variational wavefunction $|\Psi_0\rangle$ is given. In reality we find more convenient to treat $n(z)$ as an additional variational parameter, and constrain $|\Psi_0\rangle$ to span all paramagnetic Slater determinants that have a fixed local charge density $n(z)$. The average value of (1) within the Gutzwiller approximation is accordingly given by^{41,42}

$$E = \frac{\langle \Psi | H | \Psi \rangle}{\langle \Psi | \Psi \rangle} \simeq \sum_{\mathbf{R}} U_{\mathbf{R}} \frac{n(z)^2}{4} \lambda_2(z)^2 + \epsilon_{\mathbf{R}} n(z) - \sum_{\langle \mathbf{R}\mathbf{R}' \rangle_{\sigma}} t_{\mathbf{R}\mathbf{R}'} R(z) R(z') \langle \Psi_0 | c_{\mathbf{R}\sigma}^{\dagger} c_{\mathbf{R}'\sigma} + H.c. | \Psi_0 \rangle, \quad (8)$$

where

$$R(z) = \left(1 - \frac{n(z)}{2}\right) \lambda_0(z) \lambda_1(z) + \frac{n(z)}{2} \lambda_1(z) \lambda_2(z), \quad (9)$$

plays the role of a wavefunction renormalization factor, whose square can be regarded as the actual layer-dependent quasiparticle weight, $Z(z) = R^2(z)$. Because of Eqs. (6), (7) and (9), one can express

$$\lambda_n(z) = \lambda_n [R(z), n(z)],$$

as functional of the two variational functions $R(z)$ and $n(z)$. Furthermore, the single-particle wavefunctions that define the Slater determinant $|\Psi_0\rangle$ can be chosen, for a slab geometry, to have the general expression

$$\phi_{\epsilon \mathbf{k}_{\parallel}}(\mathbf{R}) = \sqrt{\frac{1}{A}} e^{i \mathbf{k}_{\parallel} \cdot \mathbf{R}} \phi_{\epsilon \mathbf{k}_{\parallel}}(z),$$

where A is the number of sites per layer and \mathbf{k}_{\parallel} the momentum in the x - y plane. The minimum of E , Eq. (8), can then be obtained by searching for saddle points with respect to the variational parameters $R(z)$, $n(z)$ and $\phi_{\epsilon\mathbf{k}_{\parallel}}(z)$, the latter subject to the constraint

$$\frac{2}{A} \sum^{\text{occupied}} |\phi_{\epsilon\mathbf{k}_{\parallel}}(z)|^2 = n(z),$$

the sum running over all occupied states in the Slater determinant.

$$\epsilon \phi_{\epsilon\mathbf{k}_{\parallel}}(z) = R(z)^2 \epsilon_{\mathbf{k}_{\parallel}}(z) \phi_{\epsilon\mathbf{k}_{\parallel}}(z) - R(z) \sum_{p=\pm 1} t(z, z+p) R(z+pa) \phi_{\epsilon\mathbf{k}_{\parallel}}(z+pa), \quad (10)$$

$$R(z) = \frac{4\sqrt{1-R(z)^2}}{U(z)A} \sum_{\epsilon\mathbf{k}_{\parallel}}^{\text{occupied}} \left[-2R(z)\epsilon_{\mathbf{k}_{\parallel}}(z)\phi_{\epsilon\mathbf{k}_{\parallel}}(z)^2 + \phi_{\epsilon\mathbf{k}_{\parallel}}(z) \sum_{p=\pm a} t(z, z+p)R(z+pa)\phi_{\epsilon\mathbf{k}_{\parallel}}(z+pa) \right], \quad (11)$$

where $\epsilon_{\mathbf{k}_{\parallel}}(z) = -2t(z)(\cos k_x a + \cos k_y a)$. The first equation has the form of a Schrödinger equation which the single-particle wavefunctions $\phi_{\epsilon\mathbf{k}_{\parallel}}(z)$ must satisfy, the quasiparticle hopping now depending parametrically on $R(z)$. The second equation has been intentionally cast in the form of a map $R_{j+1}(z) = F[R_j(z), R_j(z+a), R_j(z-a)]$ whose fixed point we have verified to coincide with the actual solution of (11) in the parameter region of interest.

In spite of the various assumptions above, solving this saddle point problem remains in principle formidable. Fortunately, Eqs. (10) and (11) can in fact be solved relatively easily, by the following iterative procedure. First solve the Schrödinger equation at fixed $R_j(z)$; next find the new $R_{j+1}(z)$ using the old $R_j(z)$ and the newly determined wavefunctions $\phi_{\epsilon\mathbf{k}_{\parallel}}(z)$. With the new $R_{j+1}(z)$, repeat the above steps and iterate until some desired level of convergence is reached. Because of the large number of variational parameters, this iterative scheme is much more efficient than – but fully equivalent to – a direct minimization of E , Eq. (8). Away from particle-hole symmetry, the saddle point equations get more involved but the solution can be obtained along the same lines.

Before concluding, we recall for future use the Gutzwiller approximation results for the Mott transition at particle-hole symmetry in the homogeneous case, $\epsilon_{\mathbf{R}} = 0$, $t_{\mathbf{R}\mathbf{R}'} = t$ and $U_{\mathbf{R}} = U$, i.e. when the variational parameters $\lambda_n(z)$ are z -independent. In this case, the solution of Eqs. (10) and (11) is trivial. The critical values $U = U_{\text{crit}}$ at the Mott transition are $U_{\text{crit}} = 32t/\pi$ (for a linear chain), $U_{\text{crit}} = 128t/\pi^2$ (for a square lattice), $U_{\text{crit}} = 16t$ (for a cubic lattice). The quasiparticle weight Z in terms of the electron-electron interaction U has the

Considerable simplifications arise if we further assume a bipartite lattice with a Hamiltonian (1) invariant under the particle-hole transformation

$$c_{\mathbf{R}\sigma} \rightarrow \sigma (-1)^R c_{\mathbf{R}-\sigma}^{\dagger},$$

where $(-1)^R$ is $+1$ on one sublattice and -1 on the other. This symmetry requires $\epsilon_{\mathbf{R}} = 0$ in (1) and implies $n(z) = 1$ hence $\lambda_0(z) = \lambda_2(z)$ and $\lambda_1(z)^2 = 2 - \lambda_0(z)^2$. In this case the saddle point is simply obtained by solving the coupled equations

simple expression

$$Z = R^2 = 1 - \frac{U^2}{U_{\text{crit}}^2}, \quad (12)$$

linearly vanishing at the Mott transition.¹⁵

III. INTERFACES IN THE 3D HUBBARD MODEL: RESULTS

We use the technique just exposed to study 3D simple cubic Hubbard model interfaces in a slab geometry with in-plane (xy) translational symmetry and layer(z)-dependent Hamiltonian parameters. We assume for simplicity particle-hole symmetry and site-independent hoppings $t_{\mathbf{R}\mathbf{R}'} = t$ throughout, so that the only source of inhomogeneity is a layer-dependent $U(z)$. Therefore the minimization procedure amounts to solve the coupled equations (10) and (11) with constant hoppings. Technically, we diagonalized the in-plane k -dependent Hamiltonian (10) at every point of a Monkhorst-Pack k -grid⁴³. The two-dimensional grid used was 32×32 , chosen so as to yield well converged values not just for the quasiparticle weight (for which a 4×4 grid was sufficient) but also for the hopping matrix element for the geometries and interaction parameters considered. At every iteration j , we choose for the convergence indicator

$$Q_j = \frac{1}{N} \left(\sum_{i=0}^N |Z_j(i) - Z_{j-1}(i)| \right) \quad (13)$$

a threshold of 10^{-6} . This corresponds to a relative energy convergence of less than 10^{-7} . The calculations of the spatial dependence of the hopping matrix elements (see

appendix B) were instead performed with a denser k -grid of 64×64 k -points.

We consider the three different geometries displayed in Fig. 1:

- (a) *Correlated metal-vacuum interface*: a correlated metal ($U_{\text{bulk}} < U_{\text{crit}}$, where $U_{\text{crit}} = 16t$ is the critical value of U at the Mott transition in the cubic lattice) with a stronger correlated surface ($U_{\text{surface}} > U_{\text{crit}}$).
- (b) *Weakly correlated metal-strongly correlated metal interface*: a junction between a moderately correlated metal ($U_{\text{left}} < U_{\text{crit}}$) and a strongly correlated metal ($U_{\text{right}} \lesssim U_{\text{crit}}$).
- (c) *Metal-Mott insulator-metal double junction*: a Mott insulator $U_{\text{center}} \gtrsim U_{\text{crit}}$ or a strongly correlated metal $U_{\text{center}} \lesssim U_{\text{crit}}$ sandwiched between two moderately correlated metallic leads $U_{\text{left}} = U_{\text{right}} < U_{\text{crit}}$.

The dashed lines in the panels of Fig. 1 show the quasi-particle weight $Z(z)$ calculated for a $N = 200$ layer slab in the three geometries with the Hamiltonian parameters:

panel (a) $U_{\text{bulk}} = U(z > 1) = 15.9712t$ and $U_{\text{surface}} = U(z = 1) = 20t$. The bulk is a strongly correlated metal very close to the Mott transition, the right surface has the same U as the bulk while the left surface has a higher value well inside the Mott insulating range.

panel (b) $U_{\text{left}} = U(z \leq 100) = 15.9198t$ and $U_{\text{right}} = U(z > 100) = 15.9712t$; The left metal is much less correlated than the right metal.

panel (c) $U_{\text{right}} = U(z \leq 80) = U_{\text{left}} = U(z > 120) = 15.9198t$ and $U_{\text{center}} = U(80 < z \leq 120) = 16.0288t$. Left and right leads are moderately correlated metals, the central region is Mott insulating.

We now discuss each case separately.

A. Geometry (a): Correlated metal-vacuum interface

This is the simple surface case, $U(z > 1) = U_{\text{bulk}} < U_{\text{crit}}$ and $U(z = 1) = U_{\text{surface}} > U_{\text{crit}}$, previously studied in Ref. 38. Looking at Figs. 2 and 3, with values of $U_{\text{surf}} = 20t$, and $U_{\text{bulk}} = 9.6t$ and $U_{\text{bulk}} = 15.97118t$, respectively, we observe that:

- i) The value of $Z(z)$ at the center of the slab, close to the bulk value, decreases monotonically to zero while U_{bulk} approaches U_{crit} . Due to the finite slab thickness N , the actual value of U at which $Z(z)$ vanishes everywhere is slightly smaller than the bulk value $U_{\text{crit}} = 16t$ for an infinite system, but tends to it as N increases. In this limit, the dependence of $Z_{\text{bulk}} = Z(z = N/2)$ upon U_{bulk} is described by Eq.(12).

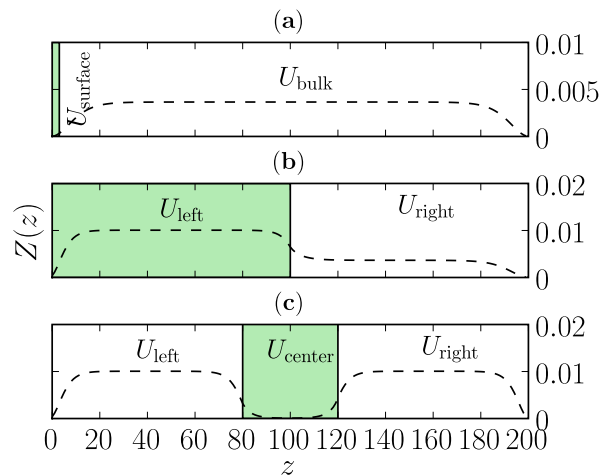


Figure 1: (Color online) The three different inhomogeneities studied in this paper: (a) free surface geometry, (b) junction between metals with different strength of correlation, (c) Mott (or strongly correlated) slab sandwiched between metallic leads (sandwich geometry). The values for U in all the three cases shown are: (a) $U_{\text{surface}} = 20t$, $U_{\text{bulk}} = 15.9712t$; (b) $U_{\text{left}} = 15.9198t$, $U_{\text{right}} = 15.9712t$; (c) $U_{\text{left}} = U_{\text{right}} = 15.9198t$, $U_{\text{center}} = 16.0288t$ (which is the case of a Mott central slab). In panel (c) the region with electron-electron interaction $U = U_{\text{center}}$ is indicated by the green-shaded area.

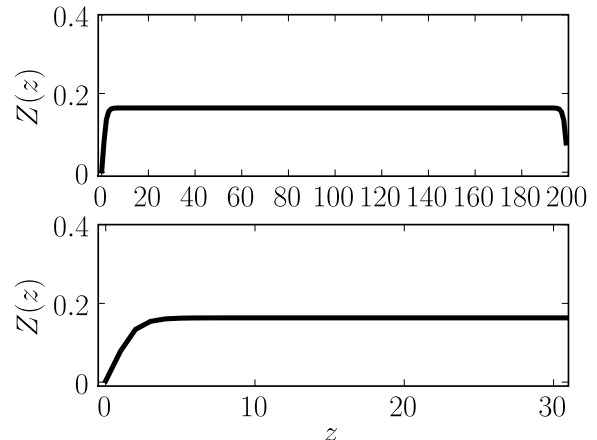


Figure 2: Spatial dependence of $Z(z)$ for $U_{\text{surf}} = 20t$ at $z = 0$ and $U_{\text{bulk}} = 14.6642t$, for any $z > 0$. The lower panel is the same as the upper one zoomed close to the surface.

- ii) $Z(z)$ decreases dramatically while approaching the surfaces, both the extra-correlated left surface $z = 1$, and the regular bulk-like one at $z = N$. In fact, within the Gutzwiller approximation, the effective interaction strength at a given site is the value of U relative to the average hopping energy at that site. The reduced surface coordination lowers the overall hopping energy of a surface site, and hence

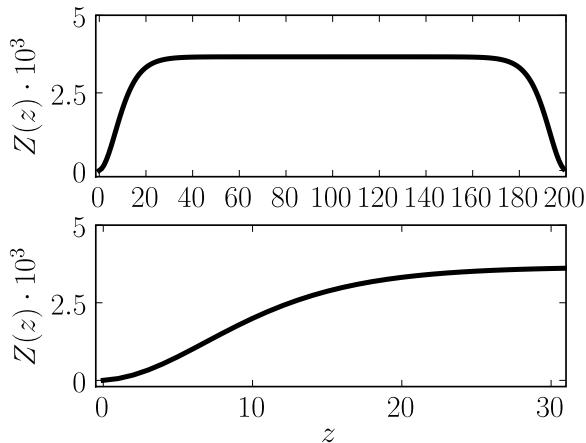


Figure 3: Same as Fig. 2, for $U_{\text{surf}} = 20t$ and $U_{\text{bulk}} = 15.9712t$.

effectively strengthens the surface interaction. The same effect would be obtained by decreasing the hopping at the surface. We note however that, so long as Z remains finite in the interior of the slab, Z remains finite, even if very small, also at the surface: there cannot be truly insulating surfaces coexisting with a metallic bulk. The reason is that, if we assume initially such an insulating surface, then simple tunneling from the underlying bulk will bring the metallic quasiparticle weight to a nonzero value, however small.

- iii) The steep decay of $Z(z)$ at the surfaces at $z = 1$ and $z = N$ gets more and more gradual as $U_{\text{bulk}} \rightarrow U_{\text{crit}}$.

As found in Ref. 38, the behavior of $R(z) = \sqrt{Z(z)}$ can be well described by an exponential

$$R(z) = R_{\text{bulk}} + (R_{\text{surf}} - R_{\text{bulk}}) e^{-(z-1)/\xi}, \quad (14)$$

where $R_{\text{bulk}} = R(z = N/2)$ and $R_{\text{surf}} < R_{\text{bulk}}$. In Appendix A we actually derive a more involved analytical expression for $R(z)$ that fits well the numerical data, see Eq. (A6). The surface value, R_{surf} , and the surface metallic quasiparticle weight $Z_{\text{surf}} = R_{\text{surf}}^2$, are much smaller than the bulk ones but, as previously mentioned, they can vanish only when R_{bulk} becomes strictly zero, for $U_{\text{bulk}} > U_{\text{crit}}$. For any $U_{\text{bulk}} < U_{\text{crit}}$, there is a surface *dead layer*³⁸, which is much less metallic than the bulk, whose thickness $\xi(U)$ depends only on bulk properties, and diverges for $U_{\text{bulk}} \rightarrow U_{\text{crit}}$ in the critical form

$$\xi \sim (U_{\text{crit}} - U_{\text{bulk}})^{-\nu}. \quad (15)$$

Therefore ξ may be identified with the correlation length characteristic of the bulk Mott transition. Numerically, we find $\nu = 0.53 \pm 0.3 \simeq 0.5$, a typical mean field critical

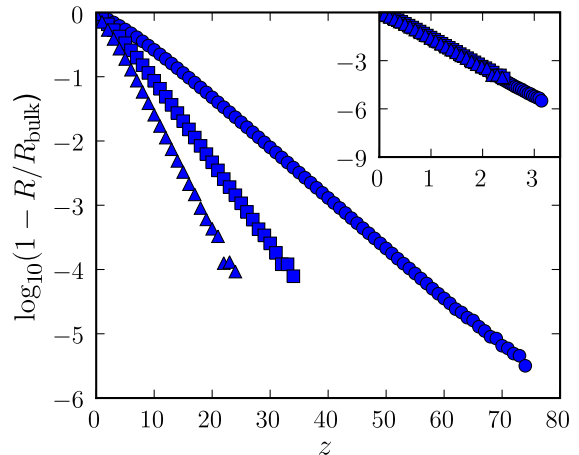


Figure 4: (Color online) Plot of $\log(1 - R/R_{\text{bulk}})$ versus z for $U = 15.97118t$ (circles), $U = 15.9198t$ (squares), $U = 15.84242t$ (triangles). In the inset the same data are plotted with respect to $z(1 - U/U_{\text{crit}})^{0.5}$.

exponent compatible with the simple Gutzwiller approximation. In Fig. 4 we plot the logarithm of the difference between R and R_{bulk} , which clearly shows the exponential decay for three values of U . In the inset of the same figure we plot the same quantity as function of a rescaled coordinate $z \rightarrow z(1 - U/U_{\text{crit}})^\nu$ with $\nu = 0.5$: all data fall on the same curve thus substantiating our statement on the U -dependence of the correlation length. Our finding of an exponential recovery of the quasiparticle weight inside the bulk in place of the expected Friedel-like power-law behavior offers a unique opportunity to experimentally access the critical properties of the Mott transition. Photoemission experiments³⁷ show that the surface depletion of metallic electron spectral weight in V_2O_3 propagates inside the interior of the sample for an anomalously large depth of many tens of Angstrom beneath the surface, in qualitative agreement with our results. Further experiments would be desirable to follow the behavior of this length scale upon approaching this and other Mott transitions and verify our prediction.

We end by noting that the calculated $Z(z)$ shows an upward curvature near the surface ($z = 0$), see Fig. 3 and also Eq. (A12) in the appendix. This is unlike earlier results obtained by the so-called linearized DMFT²⁸, displaying instead a linear growth of $Z(z)$ near the surface and very close to criticality. Besides a qualitative agreement with the upward curvature observed in photoemission,³⁷ which could be coincidental since the real V_2O_3 is much more complicated than our simple one-band Hubbard model, we do not see strong arguments of principle supporting either approaches. Both Gutzwiller and linearized DMFT are based on rather uncontrolled approximations. More reliable techniques, such as straight DMFT or Quantum Monte Carlo calculations on large size systems, would be needed to clarify this aspect; but this is perhaps not important enough. What is more im-

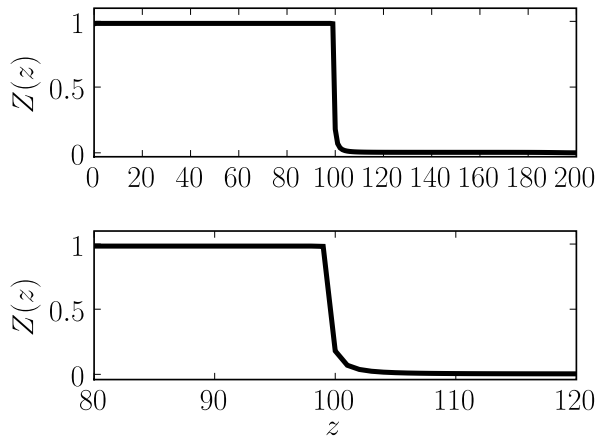


Figure 5: Spatial dependence of $Z(z)$ for $U_{\text{left}} = 2t$ and $U_{\text{right}} = 15.9712t$. The lower panel shows the same data as the upper one but closer to the interface.

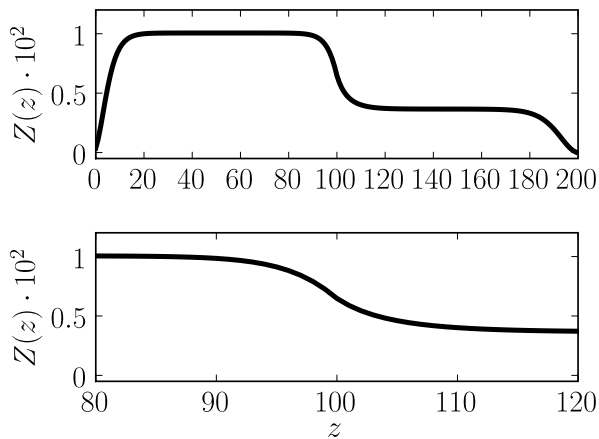


Figure 6: Same as in Fig. 5, for $U_{\text{left}} = 15.9198t$ and $U_{\text{right}} = 15.9712t$.

portant is that, just like our approach, also linearized DMFT yields, as we checked, to a length controlling the depth of the surface perturbed region that diverges at the Mott transition.

B. Geometry (b): Weakly correlated metal-strongly correlated metal interface

The junction between a metal and a Mott insulator or a strongly correlated metal was studied recently by Helmes, Costi and Rosch³⁴, who used the numerical renormalization group as DMFT impurity solver. With our simpler method we can address a broader class of interfaces, including the general case of a correlated metal-correlated metal junction, with different values of electron-electron interaction in the left (U_{left}) and right (U_{right}) leads. The

system we consider, see Fig. 1(b), is made of two blocks 100 layers each, and the junction center is at $z = N/2$. Figs. 5 and 6 show the z dependence of the quasiparticle weight for fixed $U_{\text{right}} \simeq U_{\text{crit}}$ and two different values of $U_{\text{left}} < U_{\text{right}}$. Even if $U(z)$ is changed stepwise from left to right, we find that the closer U_{left} is to U_{crit} , the smoother the function $Z(z)$ for $z < N/2$. On the right side of the junction, after a characteristic length ξ_{right} , the quasiparticle weight Z reaches exponentially its bulk value. We find for $R(z > N/2)$ a layer dependence well represented by the form (for a better fit see Eq. (A6) with the minus sign)

$$R(z) = R_{\text{right}} + (R_{\text{left}} - R_{\text{right}}) e^{-(z-N/2)/\xi_{\text{right}}}. \quad (16)$$

The dependence of ξ_{right} on U_{right} is again given by Eq. (15), i.e $\xi_{\text{right}} \propto (U_{\text{crit}} - U_{\text{right}})^{-\nu}$ ($\nu \approx 0.5$). By symmetry, the same holds in the left side too, upon interchanging the subscripts right and left.

Our results for weak U_{left} and $U_{\text{right}} \lesssim U_{\text{crit}}$ can be directly compared with those of Helmes *et al.*³⁴, who proposed that a strongly correlated slab, our right lead with $U_{\text{right}} \simeq U_{\text{crit}}$, in contact with a non interacting metal, our left lead, has a quasiparticle weight $Z(x)$ that, close to criticality, has a scaling behavior

$$x^2 Z(x) \simeq C f \left(x \left| \frac{U - U_{\text{crit}}}{U_{\text{crit}}} \right|^{1/2} \right), \quad (17)$$

where $f(0) = 1$ and x is the distance from the interface, translated in our notation $x = z - N/2$ and $U = U_{\text{right}}$. The prefactor $C \simeq 0.008$ and the asymptotic behavior $f(\zeta \rightarrow \infty) = 0.15\zeta^2$ of the scaling function were extracted by a DMFT calculation with a 40 layer correlated slab in contact with a 20 layer almost uncorrelated metal³⁴.

We show in Fig. 7 the quantity $x^2 Z(x)$ extracted by our Gutzwiller technique and plotted versus $x |1 - U/U_{\text{crit}}|^{1/2}$ for different U 's across the Mott transition value. The results are qualitatively similar to those of Ref. 34, but differs in two aspects. First of all we find that $f(\zeta)$ defined in Eq. (17) shows a plateau only when

$$z_* \ll x \ll \left| 1 - \frac{U}{U_{\text{crit}}} \right|^{-1/2},$$

where an approximate expression for the offset value z_* is given in the appendix A 1, see Eqs. (A7) and (A15). For $x \ll z_*$, $f(\zeta) \sim \zeta^2$ so that $Z(x)$ approaches its surface value at the interface. In our data the crossover between the two different regimes is clearly visible, unlike in Ref. 34. More seriously, the coefficient $C \simeq 0.08$ found by Helmes *et al.*³⁴ is almost two orders of magnitude smaller than our, which is numerically around $\simeq 0.4$. [The approximate analytical expression discussed in the appendix A give a slightly larger value of $2/3$, see (A11) and (A17)]. In the same appendix we also show that, within the linearized DMFT approach introduced by Potthoff and Nolting²⁸ one would extract yet another value

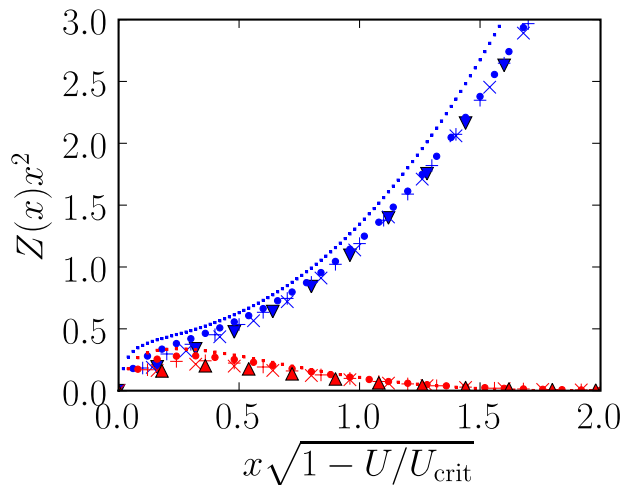


Figure 7: (Color online) Plot of $Z(x)x^2$ versus the renormalized coordinate $x\sqrt{|1-U/U_{\text{crit}}|}$ for $U < U_{\text{crit}}$ (upper blue curves: $U = 15.7939t$ triangles, $U = 15.8424t$ crosses, $U = 15.9198t$ pluses, $U = 15.9712t$ points, $U = 15.9968t$ tiny dots) and $U > U_{\text{crit}}$ (lower blue curves: $U = 16.2571t$ triangles, $U = 16.2035t$ crosses, $U = 16.1148t$ pluses, $U = 16.0511t$ points, $U = 16.0128t$ tiny dots). This figure can be compared with the inset of Fig. 3 in reference 34

of the coefficient $C = 9/11 \sim 0.82$, of the same order as ours, and again larger than that found by Helmes *et al.*³⁴. This disagreement is not just quantitative. Mainly because of the smallness of the prefactor, Helmes and coworkers³⁴ concluded that the strongly correlated slab with $U \simeq U_{\text{crit}}$ hence $Z_{\text{bulk}} = Z(x \rightarrow \infty) \ll 1$ is very weakly affected by the proximity of the good metal, a conclusion later questioned by Zenia *et al.*³⁵, who however considered a different geometry. Our results, as well as those that could be obtained by linearized DMFT, do not allow any such drastic conclusion. Yet, since straight DMFT should be more reliable than either linearized DMFT or our Gutzwiller approach, it is likely that our $Z(x)$ is strongly overestimated and that Helmes *et al.*'s conclusions are basically correct. It seems worth investigating further this important question with full DMFT on wider slabs.

C. Geometry (c): Correlated metal-Mott insulator (Strongly correlated metal)-correlated metal double junction

In this section we consider geometry (c) of figure 1, in which a strongly correlated slab of d layers is sandwiched between two weakly correlated metal leads, a setup already studied by DMFT^{31,35}. In Figs. 8, 9 and 10 we show the layer dependence of the quasiparticle weight for different values of the interaction parameters, the Hubbard U in the leads, $U_{\text{right}} = U_{\text{left}} < U_{\text{crit}}$, and in the central slab, $U_{\text{center}} > U_{\text{crit}}$, and slab thickness d . From

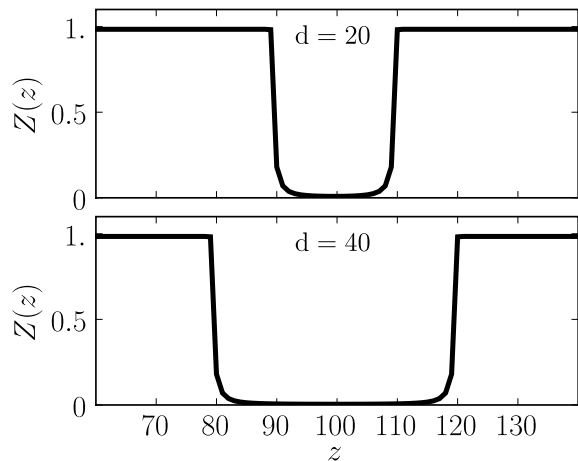


Figure 8: Spatial dependence of $Z(z)$ for $U_{\text{left}} = U_{\text{right}} = 2t$ and $U_{\text{center}} = 15.9712t$. The upper panel refers to a central region of $d = 20$ layers, while the lower panel to $d = 40$

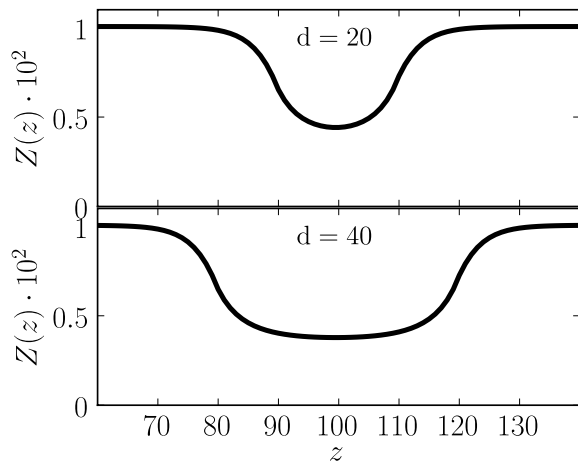


Figure 9: Same as in Fig. 8, for $U_{\text{left}} = U_{\text{right}} = 15.9198t$ and $U_{\text{center}} = 15.9712t$.

those results one can draw the following conclusions:

- For any finite thickness d , the quasiparticle weight in the central slab never vanishes, as better revealed in Figs. 11 and 12, even for $U_{\text{center}} > U_{\text{crit}}$, fed as it is by the evanescent metallic quasiparticle strength from the metallic leads. This result agrees perfectly with recent DMFT calculations³⁵.
- For $U_{\text{center}} > U_{\text{crit}}$, see Fig. 10, the minimum value Z_{min} in the central region decreases when d increases;
- The behavior of $Z(z)$ across the interface is smoother and smoother the closer and closer $U_{\text{right}} = U_{\text{left}}$ are to U_{center} .

Looking more in detail at Figs. 9, 10 and at the log-scale plots in Fig. 11 and 12, we can identify the char-

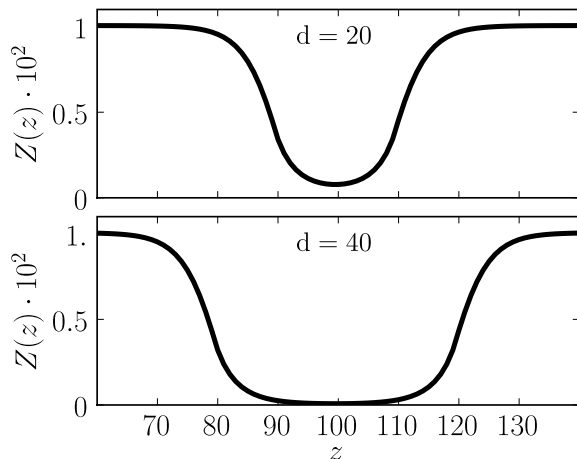


Figure 10: Same as in Fig. 8, for $U_{\text{left}} = U_{\text{right}} = 15.9198t$ and $U_{\text{center}} = 16.0288t$.

acteristic differences between a Mott insulating slab and a strongly correlated metallic slab, when sandwiched between metallic leads. In a strongly correlated metallic slab, the central quasiparticle weight ultimately settles to the self-standing value it would have in a homogeneous system with $U = U_{\text{center}} < U_{\text{crit}}$. This value is independent of the junction width and of lead correlations. On the contrary, the quasiparticle weight inside the insulating slab is completely borrowed from the leads, and strongly depends therefore on their separation and correlation. What depends strictly on the central slab interaction $U_{\text{center}} > U_{\text{crit}}$ is the quasiparticle decay length ξ_{center} from the lead to the center of the slab, which increases for increasing slab correlation according to the law $(U_{\text{center}} - U_{\text{crit}})^{-\nu}$, with $\nu \approx 0.5$, a value that matches perfectly that found in section III A

These considerations suggest that, if we look at the problem from a transport point of view, we are confronted with two completely different mechanisms. In a strongly correlated metallic central slab, ξ_{center} has the role of a screening length, exactly the same role of ξ_{right} in section III B. If instead the central slab is insulating, the meaning of ξ_{center} becomes completely different, it is now a tunneling length. No local quasiparticle peak would survive in a homogeneous Mott insulator: the residual quasiparticle peak that we find inside the central slab is therefore the evanescent lead electron wavefunction that tunnels into the slab.

A special case occurs when $U_{\text{center}} \approx U_{\text{crit}}$, i.e. right at criticality, where neither of the previous two pictures is valid. The crossover from the two opposite exponential decays describing either screening or tunneling is characterized by the absence of any characteristic length, which implies a power law variation of the quasiparticle strength upon the slab width d

$$Z_{\text{min}}(d) \sim \frac{1}{d^2} + O\left(\frac{1}{d^3}\right). \quad (18)$$

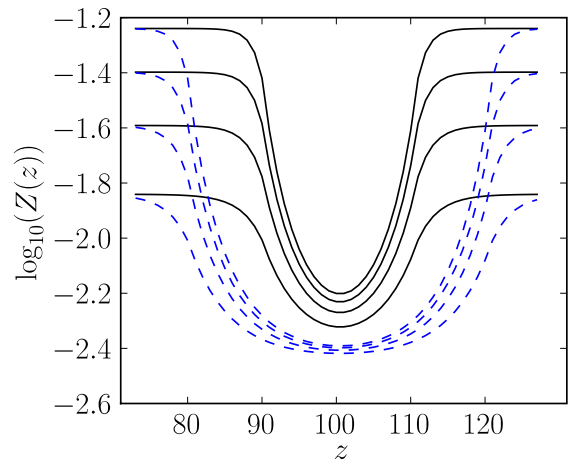


Figure 11: (Color online) Logarithm of the quasiparticle weight Z as a function of layer index z for a 20-sites wide (solid line) and 40-sites wide (dashed line) strongly correlated metallic slab $U = 15.9712t < U_{\text{crit}}$ sandwiched between two weakly correlated metal leads (with $U = 15.88438t, 15.79388t, 15.67674t, 15.53236t$). The entire system is 200-sites wide; the interfaces between the leads and the slab are at $z = 80$ and $z = 120$ for the 40-sites wide slab and $z = 90$ and $z = 110$ for the 20-sites wide slab. The figure shows that for increasing slab width the quasiparticle weight goes to a value that is independent of lead correlation.

We find that the leading $1/d^2$ behavior is, within our accuracy, independent of the specific properties of the metallic leads, while the subleading terms do depend on them, see Fig. 14. A simple analytical justification of the critical $1/d^2$ behavior is provided in appendix A.

IV. CONCLUSIONS

In this work we have studied how the spatial inhomogeneity of interfaces affects the physics of a strongly correlated electron system. To address this problem, we extended the conventional Gutzwiller approximation technique to account for inhomogeneous Hamiltonian parameters. Moreover, to efficiently cope with the larger number of variational parameters in comparison with the homogeneous case, we derived iterative equations fully equivalent to the saddle point equations that identify the optimal variational solution, similarly to what is commonly done within unrestricted Hartree-Fock or *ab initio* LDA calculations. These iterative equations can be solved without much effort for very large system sizes; an advantage with respect to more rigorous approaches, like e.g. DMFT calculations, which are numerically feasible only for small systems.

We have applied the method to various interface geometries in three dimensions; specifically the interface of a strongly correlated metal with the vacuum, the interface between two differently correlated metals and

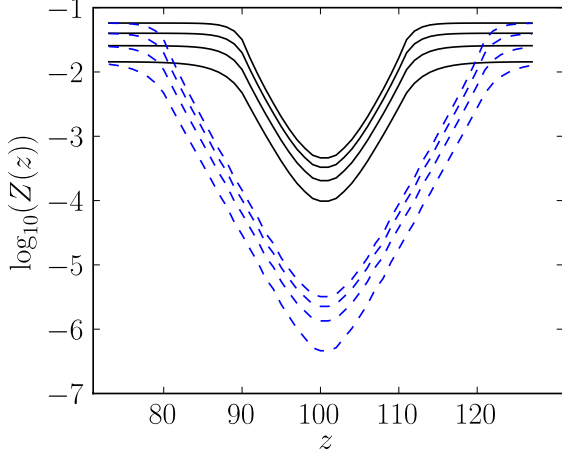


Figure 12: (Color online) Same as in Fig. 11, but the central layers have now $U = 16.1148 > U_{\text{crit}}$. In this case the quasiparticle weight at the center of the junction is strongly dependent both on barrier width and on the strength of electron correlation in the leads. The central layer remains metallic for arbitrary values of $U > U_{\text{crit}}$, but its quasiparticle weight decreases exponentially with the slab width.

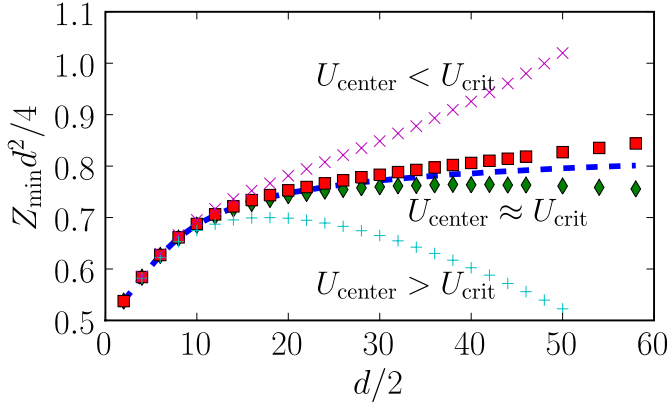


Figure 13: (Color online) Numerical results for $Z_{\text{min}}d^2/4$ and $U = 15.999t$ (crosses), $16t$ (squares), $16.0002t$ (dashed line), $16.0004t$ (diamonds), $16.002t$ (pluses) for the sandwich geometry with $U_{\text{left}} = U_{\text{right}} = 2t$. The constant value approached for $U = 16.0002t \approx U_{\text{crit}}$ and large junction width should be compared to the one we find in Eq. (A25).

the junction between two weakly correlated metals sandwiched by a strongly correlated slab. All these geometries had been already studied by DMFT^{27,28,31,32,33,34,35,36}, which allowed us to directly compare our results with more rigorous ones, thus providing a test on the quality of our approximation, which is then applied to much larger sizes.

Our main result is that the effects of an interface decay exponentially in the interior of a strongly correlated system on a very long length-scale proportional to the correlation length of the incipient Mott transition, a bulk property independent upon the details of the interface.³⁸

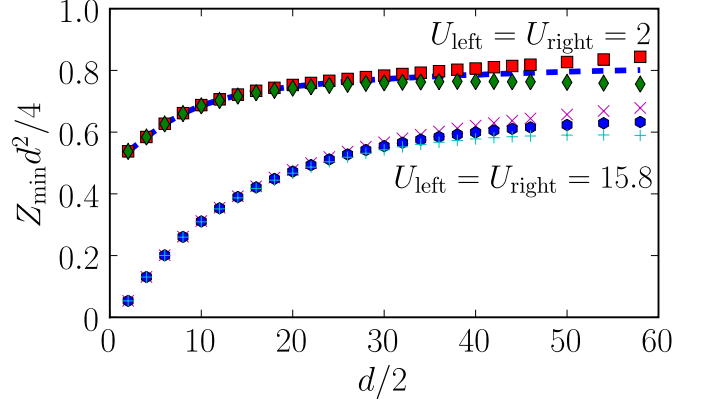


Figure 14: (Color online) Numerical results for $Z_{\text{min}}d^2/4$ for $U_{\text{left}} = U_{\text{right}} = 2t$ [$U_{\text{center}} = 16t$ (squares), $16.0002t$ (dashed line), $16.0004t$ (diamonds)], and for $U_{\text{left}} = U_{\text{right}} = 15.8t$ [$U_{\text{center}} = 16.0002t$ (crosses), $16.0004t$ (hexagons), $16.0006t$ (pluses)]. The stronger lead correlation in the lower curves pushes the plateau of the function $Z_{\text{min}}d^2/4$ towards larger values of d .

In particular, at the surface of a strongly correlated metal we find a strong suppression of the metallic properties, e.g. of the quasiparticle weight, that persists on a large depth controlled by the Mott transition correlation length, a “dead layer”³⁸ appearing because the surface is effectively more correlated than the bulk and consistent with photoemission experiments.³⁷ Conversely, metallic features from a metal lead penetrate inside a Mott insulator within a depth that, once again, diverges on approaching the Mott transition. As a consequence, a conducting channel always exists inside a Mott insulating slab contacted to two metallic leads, in agreement with recent DMFT analyses³⁵, implying a finite conductance at zero bias and temperature that decays fast on increasing both external parameters on an energy scale exponentially small in the length of the slab in units of the Mott transition correlation length.

The method that we have developed is very simple and flexible, so it can in principle be applied to a variety of realistic situations of current interest, not only for studying interfaces but also for more general inhomogeneities, as those arising by impurities or other defects, and can easily incorporate additional features like magnetism, which we have disregarded throughout this work.

Acknowledgments

The work was supported by the Italian Ministry of University and Research, through a PRIN-COFIN award. The environment provided by the independent ESF project CNR-FANAS-AFRI was also useful.

Appendix A: ANALYTICAL EXPRESSIONS NEAR CRITICALITY

In this appendix, we show how to derive simple analytical expressions for the layer dependence of the quasiparticle residue near criticality. We assume a three dimensional slab geometry with constant hopping but inhomogeneous interaction $U(z)$ and with particle-hole symmetry. We define as $2\epsilon_{\parallel}(z)$ and $2\epsilon_{\perp}(z - 1/2)$ the average over the uncorrelated Slater determinant $|\Psi_0\rangle$ of the hopping energy per bond within layer z and between layers z and $z - 1$, respectively. With these definitions, the equation (11) can be written as

$$0 = 2R(z) \left(4\epsilon_{\parallel}(z) + \epsilon_{\perp}(z - 1/2) + \epsilon_{\perp}(z + 1/2) \right) + \left(\epsilon_{\perp}(z - 1/2) + \epsilon_{\perp}(z + 1/2) \right) \left(R(z + 1) + R(z - 1) - 2R(z) \right) + \left(\epsilon_{\perp}(z + 1/2) - \epsilon_{\perp}(z - 1/2) \right) \left(R(z + 1) - R(z - 1) \right) + \frac{U(z)}{4} \frac{R(z)}{\sqrt{1 - R^2(z)}}. \quad (\text{A1})$$

Near criticality, we expect that the layer dependence must appear as a dependence upon the scaling variable z/ξ , and, since $\xi \gg 1$, it becomes allowed to regard z/ξ as a continuous variable and expand (A1) in the leading gradients. Because of the interface, both $\epsilon_{\parallel}(z)$ and $\epsilon_{\perp}(z - 1/2)$ must acquire a Friedel-like z -dependence. However, as shown explicitly in Fig. 15, $\epsilon_{\parallel}(z)$ and $\epsilon_{\perp}(z - 1/2) + \epsilon_{\perp}(z + 1/2)$ vary appreciably only close to the interfaces, while $\epsilon_{\perp}(z - 1/2) - \epsilon_{\perp}(z + 1/2)$ is negligible. Indeed, as discussed in more detail in the Appendix B, the amplitude of the Friedel's oscillations is strongly reduced near criticality, while the period stays invariant, so that it is legitimate to neglect the z dependence of $\epsilon_{\parallel}(z)$ and $\epsilon_{\perp}(z \pm 1/2)$ and use for them their large- z bulk values, ϵ_{\parallel} and ϵ_{\perp} .

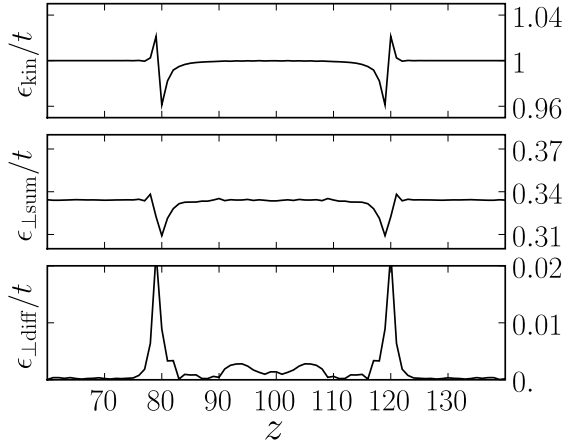


Figure 15: Upper panel, plot ϵ_{kin}/t for the sandwich geometry (c) with 40 central layers, $U_{left} = U_{right} = 2t$ and $U_{center} = 15.9712t$. The value deviates by 2 to 4% from the value it would have in a homogeneous system ($\tilde{\epsilon}_{kin} = t$). Middle panel, plot of $\epsilon_{\perp sum} = \epsilon_{\perp}(z + 1/2) + \epsilon_{\perp}(z - 1/2)$. Lower panel, plot of $\epsilon_{\perp diff} = \epsilon_{\perp}(z + 1/2) - \epsilon_{\perp}(z - 1/2)$

geneous interaction $U(z)$ and with particle-hole symmetry. We define as $2\epsilon_{\parallel}(z)$ and $2\epsilon_{\perp}(z - 1/2)$ the average over the uncorrelated Slater determinant $|\Psi_0\rangle$ of the hopping energy per bond within layer z and between layers z and $z - 1$, respectively. With these definitions, the equation (11) can be written as

Noting that the average hopping energy per site in the homogeneous case is $\epsilon_{kin} = 4\epsilon_{\parallel} + 2\epsilon_{\perp}$, the above Eq. (A1) can be written in the continuous limit as

$$2R(z)\epsilon_{kin} + \frac{U}{4} \frac{R(z)}{\sqrt{1 - R^2(z)}} + 2\epsilon_{\perp} \frac{\partial^2 R(z)}{\partial z^2} = 0, \quad (\text{A2})$$

where we take the bulk value $U(z) = U$, since its variation is limited to a single layer. Eq. (A2) admits an integral of motion, namely

$$E = \epsilon_{\perp} \left(\frac{\partial R(z)}{\partial z} \right)^2 + \epsilon_{kin} R^2(z) + \frac{U}{4} \left(1 - \sqrt{1 - R^2(z)} \right) \equiv \epsilon_{\perp} \left(\frac{\partial R(z)}{\partial z} \right)^2 + E[R(z)], \quad (\text{A3})$$

where $E[R(z)]$ is the Gutzwiller variational energy for a homogeneous system calculated at fixed $R = R(z)$, i.e. not the optimized one. The constant of motion E must be chosen to correspond to $E[R(z_0)] = E[R_0]$, where z_0 is the layer coordinate at which we expect vanishing derivative. In a single interface, we expect that $R(z)$ will reach a constant value only asymptotically far from the interface, i.e. $z_0 \rightarrow \infty$, where R_0 tends to its bulk value

$$R_0 = \sqrt{1 - u^2},$$

and $E[R_0]$ to the optimized energy in a homogeneous system, i.e.

$$E = E[R_0] = -\frac{U_{crit}}{8} (1 - u)^2 \theta(1 - u),$$

with $u = U/U_{crit}$ and $U_{crit} = -8\epsilon_{kin}$, in the Gutzwiller approximation. In the case of a correlated slab sandwiched between two metal leads, we expect that $R(z)$ will reach a minimum somewhere at midway between the two interfaces. If the leads are identical, the minimum occurs

right in the middle, so that R_0 becomes an unknown parameter that has to be fixed by imposing that the actual solution $R[z, R_0]$, which depends parametrically on R_0 , has a vanishing slope $\partial_z R[z, R_0] = 0$ for z in the middle of the slab.

With the same definitions as above,

$$E[R(z)] = -\frac{U_{\text{crit}}}{8} R^2(z) + \frac{U_{\text{crit}}}{4} u \left(1 - \sqrt{1 - R^2(z)}\right).$$

Since in a homogeneous cubic lattice $\epsilon_{\perp} = \epsilon_{\text{kin}}/6 = -U_{\text{crit}}/48$, Eq. (A3) can be rewritten as

$$\frac{1}{6} \left(\frac{\partial R(z)}{\partial z}\right)^2 = R_0^2 + 2u \left(1 - \sqrt{1 - R_0^2}\right) - R^2(z) + 2u \left(1 - \sqrt{1 - R^2(z)}\right), \quad (\text{A4})$$

where

$$R_0^2 + 2u \left(1 - \sqrt{1 - R_0^2}\right) = (1 - u)^2 \theta(1 - u), \quad (\text{A5})$$

in the case of a single interface. The pre-factor 6 of the $(\partial R(z)/\partial z)^2$ comes from the homogeneous relation $\epsilon_{\text{kin}}/\epsilon_{\perp} = 6$. As we shall see, the numerical data can be better interpreted if $\epsilon_{\text{kin}}/\epsilon_{\perp}$ is considered as a free fitting parameter

The differential equation (A4) controls the z -dependence of $R(z > 0)$, hence of the quasiparticle residue $Z(z) = R^2(z)$, assuming that the interface affects only the boundary condition $R(z = 0) = R_{\text{surf}}$. Therefore, a surface less correlated than the bulk should be described by (A4) with $R_{\text{surf}} > R_{\text{bulk}} = \sqrt{1 - u^2} \theta(1 - u)$, while by $R_{\text{surf}} < R_{\text{bulk}}$ the opposite case, as for instance the interface with the vacuum of section III A.

We now consider separately the case of a single junction and of the double junction, with either metallic or insulating bulk.

1. Single interface with metallic bulk: $u \leq 1$

In the case of a single interface, Eq. (A5) with $u \leq 1$ has to be used. The differential equation (A4) reads

$$\frac{1}{6} \left(\frac{\partial R(z)}{\partial z}\right)^2 = \left(\sqrt{1 - R^2(z)} - u\right)^2,$$

hence

$$\frac{\partial R(z)}{\partial z} = \sqrt{6} \left(\sqrt{1 - R^2(z)} - u\right),$$

namely

$$\int_{R_{\text{surf}}}^{R(z)} \frac{dR}{\sqrt{1 - R^2} - u} = \sqrt{6} z.$$

This integral equation can be solved exactly, leading to the implicit formula

$$\begin{aligned} \sqrt{6} z &= \int_{\arcsin R_{\text{surf}}}^{\arcsin R(z)} \frac{\cos x dx}{\cos x - u} \\ &= \arcsin R(z) - \arcsin R_{\text{surf}} \\ &+ \frac{u}{\sqrt{1 - u^2}} \tanh^{-1} \left(\frac{R(z) R_{\text{bulk}}}{1 - \sqrt{(1 - R_{\text{bulk}}^2)(1 - R^2(z))}} \right) \\ &- \frac{u}{\sqrt{1 - u^2}} \tanh^{-1} \left(\frac{R_{\text{surf}} R_{\text{bulk}}}{1 - \sqrt{(1 - R_{\text{bulk}}^2)(1 - R_{\text{surf}}^2)}} \right). \end{aligned}$$

Close to criticality, $u \simeq 1$, one can neglect the arcsines in the rhs and find the explicit expression

$$R(z) = \frac{R_{\text{bulk}} \sinh \zeta}{\cosh \zeta \pm \sqrt{1 - R_{\text{bulk}}^2}}, \quad (\text{A6})$$

where the plus sign refers to the case $R_{\text{surf}} < R_{\text{bulk}}$, and the minus sign to the opposite case, and

$$\begin{aligned} \zeta &= \sqrt{6(1 - u^2)} z \\ &+ \tanh^{-1} \left(\frac{R_{\text{surf}} R_{\text{bulk}}}{1 - \sqrt{(1 - R_{\text{bulk}}^2)(1 - R_{\text{surf}}^2)}} \right) \\ &\equiv \sqrt{6} R_{\text{bulk}} (z + z_*). \end{aligned} \quad (\text{A7})$$

This solution provides a definition of the correlation length for $u \lesssim 1$

$$\xi = \frac{1}{\sqrt{6(1 - u^2)}} \simeq 0.289 \left(\frac{U_{\text{crit}}}{U_{\text{crit}} - U} \right)^{1/2}, \quad (\text{A8})$$

quite close to the DMFT value.³⁴ We note that, for $\zeta \gg 1$, Eq. (A6) becomes

$$R(z \rightarrow \infty) \simeq R_{\text{bulk}} \left(1 \mp \sqrt{1 - R_{\text{bulk}}^2} e^{-\zeta}\right),$$

therefore

$$Z(z) = R^2(z) \simeq Z_{\text{bulk}} \left(1 \mp 2\sqrt{1 - R_{\text{bulk}}^2} e^{-x/\xi}\right), \quad (\text{A9})$$

tends exponentially to its bulk value on a length scale ξ , from below or above according to $R_{\text{surf}} \lessgtr R_{\text{bulk}}$, respectively.

Near criticality, i.e. $R_{\text{bulk}} = \sqrt{1 - u^2} \ll 1$, Eq. (A6) becomes

$$R(z) \simeq R_{\text{bulk}} \coth \frac{\zeta}{2}, \quad (\text{A10})$$

so that

$$(z + z_*)^2 Z(z) = (z + z_*)^2 R(z)^2$$

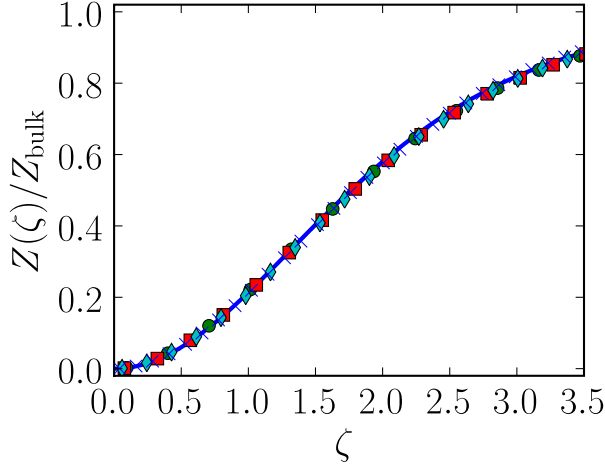


Figure 16: (Color online) Numerical results for $Z(z)$ in the surface geometry, with $U = 15.9872t$ (crosses), $15.9712t$ (diamonds), $15.9487t$ (squares), $15.9198t$ (circles). The solid curve is $\tanh^2(\zeta/2)$, i.e. $R^2(\zeta)$ as defined in Eq. (A6) (with plus sign) and expanded to first order in $R_{\text{bulk}} \ll 1$. In order to define ζ the same expansion has been carried out in Eq. (A7), where we set the quantity $\epsilon_{\text{kin}}/\epsilon_{\perp}$ equal to 9.427 instead of 6, in order to fit the numerical data.

$$= \frac{4}{6} \left(\frac{1}{4} \zeta^2 \coth^2 \frac{\zeta}{2} \right) \equiv \frac{2}{3} f_{u < 1}(\zeta), \quad (\text{A11})$$

shows a simple scaling behavior³⁴. The scaling function $f_{u < 1}(\zeta)$ that we find has the asymptotic behavior: $f_{u < 1}(0) = 1$ and $f_{u < 1}(\zeta \rightarrow \infty) \simeq \zeta^2/4$.

Another case of interest is that of the interface with vacuum discussed in section III A. Here $R_{\text{surf}} \ll 1$ hence from Eq. (A7) it follows that

$$z_* \simeq \frac{R_{\text{surf}}}{\sqrt{6}(1-u)} \ll 1.$$

Away from criticality and for $\zeta \ll 1$, which is allowed since $z_* \ll 1$, we find through (A6) with the plus sign that

$$R(z) \simeq \sqrt{6} (1-u) (z + z_*),$$

so that

$$Z(z) \simeq 6 (1-u)^2 (z + z_*)^2, \quad (\text{A12})$$

showing that the quasiparticle residue approaches its surface value with a finite curvature.

In Fig. 16 and Fig. 17 we show that rescaled numerical data for an interface between a 200-layer-wide correlated metal slab and the vacuum and for a junction between a weakly correlated metal and a strongly correlated metal.

It is easy to fit the numerical data with the function $R^2(z)$ displayed in Eq. (A7) by tuning just one parameter, which, as discussed above, is the value of $\epsilon_{\text{kin}}/\epsilon_{\perp}$ (equal to 6 in the homogeneous problem). The fact that the ideal theoretical result, relying on homogeneous values for hopping and kinetic energy, fits the numerical data with just a single tunable parameter, is a pleasant feature.

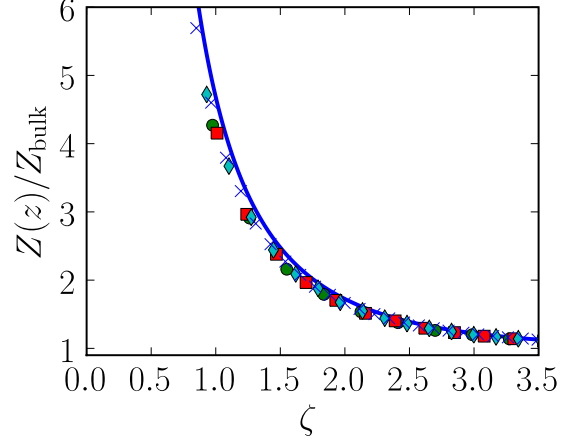


Figure 17: (Color online) Numerical results for $Z(z)$ in the single junction geometry with metallic bulk, the position of the junction is chosen as the origin for the spatial coordinate, the metal on the left side is very weakly correlated ($U = 2t$); the values for U on the right side are the same of Fig. 16. The solid curve is now the function $1/\tanh^2(\zeta/2)$, i.e. the second power of Eq. (A6) (with minus sign) expanded to first order in R_{bulk} . As in Fig. 16, the definition of ζ has been obtained from Eq. (A7) by expanding to first order in R_{bulk} . The value of $\epsilon_{\text{kin}}/\epsilon_{\perp}$ that fits the data is now 8.254.

2. Single interface with insulating bulk: $u \geq 1$

In this case the equation (A4) using (A5) with $u \geq 1$ reads

$$\frac{1}{6} \left(\frac{\partial R(z)}{\partial z} \right)^2 = -R^2(z) + 2u \left(1 - \sqrt{1 - R^2(z)} \right), \quad (\text{A13})$$

leading to

$$\int \frac{dR}{\sqrt{2u - R^2 - 2u\sqrt{1 - R^2}}} = -\sqrt{6} \int dz,$$

where we have assumed that on the surface R_{surf} is finite and decay in the bulk, so that the derivative is negative. The above integral equation can be solved too, with an implicit solution

$$\begin{aligned}
-\sqrt{6(u-1)}z &= 2\sqrt{u-1} \arcsin\left(\frac{\cos y(z)}{\sqrt{u}}\right) - 2\sqrt{u-1} \arcsin\left(\frac{\cos y_{\text{surf}}}{\sqrt{u}}\right) \\
&\quad - \tanh^{-1}\left(\frac{\sqrt{u-1} \cos y(z)}{\sqrt{u - \cos^2 y(z)}}\right) + \tanh^{-1}\left(\frac{\sqrt{u-1} \cos y_{\text{surf}}}{\sqrt{u - \cos^2 y_{\text{surf}}}}\right)
\end{aligned}$$

where $R(z) = \sin 2y(z)$, $R_{\text{surf}} = \sin 2y_{\text{surf}}$. As before the arcsines can be neglected near criticality to obtain the explicit solution

$$R^2(z) = 1 - \left(1 - \frac{2(u-1)}{u \cosh^2 \zeta - 1}\right)^2, \quad (\text{A14})$$

with

$$\begin{aligned}
\zeta &= \sqrt{6(u-1)}z + \tanh^{-1}\left(\frac{\sqrt{u-1} \cos y_{\text{surf}}}{\sqrt{u - \cos^2 y_{\text{surf}}}}\right) \\
&\equiv \sqrt{6(u-1)}(z + z_*). \quad (\text{A15})
\end{aligned}$$

In the case of an insulating bulk, the correlation length defined through (A16) is therefore

$$\xi = \frac{1}{\sqrt{6(u-1)}} \simeq 0.408 \left(\frac{U_{\text{crit}}}{U - U_{\text{crit}}}\right)^{1/2}, \quad (\text{A16})$$

with a different numerical prefactor, actually a $\sqrt{2}$ greater, with respect to the metallic bulk (A8).

Near criticality, $u \gtrsim 1$,

$$R(z)^2 = Z(z) \simeq \frac{4(u-1)}{\sinh^2 \zeta},$$

so that, as before,

$$\begin{aligned}
(z + z_*)^2 Z(z) &= \frac{4}{6} \left(\frac{\zeta^2}{\sinh^2 \zeta}\right) \\
&\equiv \frac{2}{3} f_{u>1}(\zeta), \quad (\text{A17})
\end{aligned}$$

has a scaling behavior with $f_{u>1}(0) = 1$ and

$$f_{u>1}(\zeta \rightarrow \infty) \simeq 4\zeta^2 e^{-2\zeta}.$$

3. Double junction

We assume for simplicity a slab of length $2L$ in contact with two leads. In this case we need to use Eq. (A4) with R_0 a parameter that has to be fixed by imposing that the solution $R(z)$ becomes R_0 at some z_0 within the slab. If we assume that both leads are less correlated than the slab, then $R(z)$ always decreases moving away from any of the two interfaces, and we can determine R_0 by imposing either of the two following conditions:

$$\int_{R_{\text{surf}}^<}^{R_0} \frac{dR}{\sqrt{R_0^2 + 2u\sqrt{1-R_0^2} - R^2 - 2u\sqrt{1-R^2}}} = -\sqrt{6}z_0, \quad (\text{A18})$$

$$\int_{R_0}^{R_{\text{surf}}^>} \frac{dR}{\sqrt{R_0^2 + 2u\sqrt{1-R_0^2} - R^2 - 2u\sqrt{1-R^2}}} = \sqrt{6}(2L - z_0), \quad (\text{A19})$$

where $R_{\text{surf}}^<$ and $R_{\text{surf}}^>$ are the values of $R(z)$ at the left and right surfaces, respectively. Taking the difference

(A19) minus (A18) we find

$$\sqrt{6}2L = \left(\int_{R_0}^{R_{\text{surf}}^>} + \int_{R_0}^{R_{\text{surf}}^<}\right) \frac{dR}{\sqrt{R_0^2 + 2u\sqrt{1-R_0^2} - R^2 - 2u\sqrt{1-R^2}}}, \quad (\text{A20})$$

which has to be solved to find R_0 as function of the other parameters. Once R_0 is found, one can determine z_0 . In order to simplify the calculations, we will assume two

identical leads, i.e. $R_{\text{surf}}^< = R_{\text{surf}}^> = R_{\text{surf}}$, so that $z_0 = L$ and (A20) becomes

$$\sqrt{6}L = \int_{R_0}^{R_{\text{surf}}} \frac{dR}{\sqrt{R_0^2 + 2u\sqrt{1-R_0^2} - R^2 - 2u\sqrt{1-R^2}}} = \frac{2}{\sqrt{(a-c)(b-d)}} \left[(c-b) \Pi \left(\phi, \frac{c-d}{b-d}, k \right) + b F(\phi, k) \right], \quad (\text{A21})$$

with parameters $a > b > c > u \geq d$. The last expression can be derived easily after the change of variable $R = \sqrt{1-x^2}$, and seemingly $R_0 = \sqrt{1-x_0^2}$ and $R_{\text{surf}} = \sqrt{1-x_{\text{surf}}^2}$. $\Pi(\phi, n, k)$ and $F(\phi, k)$ are elliptic integrals of third and first kind, respectively

$$F(\phi, k) = \int_0^\phi \frac{dx}{\sqrt{1-k^2 \sin^2 x}},$$

$$\Pi(\phi, n, k) = \int_0^\phi \frac{dx}{(1-n \sin^2 x) \sqrt{1-k^2 \sin^2 x}},$$

and

$$\phi = \arcsin \sqrt{\frac{(b-d)(c-u)}{(c-d)(b-u)}},$$

$$k = \sqrt{\frac{(a-b)(c-d)}{(a-c)(b-d)}}.$$

The various parameters are, when $2u - x_0 \geq 1$,

$$\begin{aligned} a &= 2u - x_0, \\ b &= 1, \\ c &= x_0, \\ d &= -1, \\ u &= x_{\text{surf}}, \end{aligned}$$

so that

$$\phi = \arcsin \sqrt{\frac{2(x_0 - x_{\text{surf}})}{(x_0 + 1)(1 - x_{\text{surf}})}},$$

$$k = \sqrt{\frac{(2u - x_0 - 1)(x_0 + 1)}{4(u - x_0)}}.$$

On the contrary, if $2u - x_0 < 1$, then

$$\begin{aligned} a &= 1, \\ b &= 2u - x_0, \\ c &= x_0, \end{aligned}$$

$$\begin{aligned} d &= -1, \\ u &= x_{\text{surf}}, \end{aligned}$$

hence

$$\phi = \arcsin \sqrt{\frac{(2u - x_0 + 1)(x_0 - x_{\text{surf}})}{(x_0 + 1)(2u - x_0 - x_{\text{surf}})}},$$

$$k = \sqrt{\frac{(1 - 2u + x_0)(x_0 + 1)}{(1 - x_0)(2u - x_0 + 1)}}.$$

We rewrite

$$\begin{aligned} (c-b) \Pi \left(\phi, \frac{c-d}{b-d}, k \right) + b F(\phi, k) & \quad (\text{A22}) \\ = \int_0^\phi dx \left(\frac{d(b-c) + b(c-d) \cos^2 x}{(b-c) + (c-d) \cos^2 x} \right) \frac{1}{\sqrt{1-k^2 \sin^2 x}}, \end{aligned}$$

and note that at $x = \phi$

$$\frac{d(b-c) + b(c-d) \cos^2 \phi}{(b-c) + (c-d) \cos^2 \phi} = x_{\text{surf}} \geq 0.$$

In addition $b-c$ in both cases is very small. Indeed, for $2u - x_0 > 1$, which corresponds to an insulating slab where $R_0 = \sqrt{1-x_0^2} \rightarrow 0$ for large L , $b-c = 1-x_0 \ll 1$. In the opposite case of a weakly correlated slab, still $b-c = 2u - x_0 - x_0 \ll 1$ since $x_0 \rightarrow u$ for large L . Therefore

$$\frac{d(b-c) + b(c-d) \cos^2 x}{(b-c) + (c-d) \cos^2 x}$$

is practically constant and equal to b everywhere but close to the extreme of integration, where it fastly decays to x_{surf} . Therefore to leading order we can write

$$(c-b) \Pi \left(\phi, \frac{c-d}{b-d}, k \right) + b F(\phi, k) \simeq b F(\phi, k),$$

hence the equation to be solved becomes

$$\sqrt{6} L = \frac{2b}{\sqrt{(a-c)(b-d)}} F(\phi, k) = \frac{2b}{\sqrt{(a-c)(b-d)}} \left[K(k) - F\left(\arcsin \frac{\cos \phi}{\sqrt{1-k^2 \sin^2 \phi}}, k\right) \right], \quad (\text{A23})$$

where $K(k) = F(\pi/2, k)$ and the last expression being more convenient since $\phi \simeq \pi/2$.

In order to find x_0 as function of the other parameters, we have to consider separately three different cases.

a. Insulating off-critical behavior: $u \gg 1$

In this case $2u - x_0 > 1$. We note that k as a function of u at fixed $x_0 \simeq 1$ is equal to

$$k^2 = \frac{x_0 + 1}{4} \simeq \frac{1}{2},$$

for $u = 1$, and very rapidly increases to its asymptotic $u \gg 1$ value

$$k^2 = \frac{x_0 + 1}{2} \simeq 1.$$

Therefore (A23) is, at leading order,

$$\sqrt{6} L = \frac{1}{\sqrt{u-1}} K\left(\sqrt{\frac{1+x_0}{2}}\right) \simeq \frac{1}{2\sqrt{u-1}} \ln \frac{32}{1-x_0}.$$

Therefore, in this limit,

$$Z_0 = R_0^2 \simeq 64 e^{-\sqrt{24(u-1)} L}, \quad (\text{A24})$$

vanishes exponentially in the length of the slab.

b. Critical behavior: $u = 1$

In this case

$$k^2 = \frac{x_0 + 1}{4} \simeq \frac{1}{2},$$

hence at leading order Eq. (A23) reads

$$\sqrt{6} L = \frac{1}{\sqrt{1-x_0}} K\left(\frac{1}{\sqrt{2}}\right) = \frac{1}{4\sqrt{\pi} \sqrt{1-x_0}} \left[\Gamma\left(\frac{1}{4}\right) \right]^2,$$

from which it follows that

$$Z_0 = R_0^2 = \frac{1}{48\pi} \left[\Gamma\left(\frac{1}{4}\right) \right]^4 \frac{1}{L^2} \simeq \frac{1.146}{L^2}. \quad (\text{A25})$$

Once again we find a critical behavior $L^2 Z_0 \simeq \text{const.}$, with a sizable constant 1.146.

c. Metallic off-critical behavior: $u \ll 1$

This is the case in which $2u - x_0 < 1$ and $x_0 \simeq u$, so that

$$1 - k^2 = \frac{4(u - x_0)}{(2u - x_1 + 1)(1 - x_0)} \simeq \frac{4(u - x_0)}{1 - u^2}.$$

Therefore Eq. (A23) is

$$\sqrt{6} L \simeq \frac{u}{\sqrt{1-u^2}} \ln \frac{16}{1-k^2} = \frac{u}{\sqrt{1-u^2}} \ln \frac{4(1-u^2)}{u-x_0},$$

whose solution is

$$u - x_0 = 4(1 - u^2) e^{-\sqrt{6} \sqrt{1-u^2} L/u}.$$

Therefore, since $Z_{\text{bulk}} = 1 - u^2$, it follows that

$$Z_0 \simeq Z_{\text{bulk}} \left(1 + 8u e^{-\sqrt{6} \sqrt{1-u^2} L/u} \right). \quad (\text{A26})$$

4. Comparison with DMFT

Near the Mott transition, $U \simeq U_{\text{crit}}$, Potthoff and Noltling in Ref. 28 have introduced a set of linearized DMFT recursive equations for the layer dependent quasiparticle residue. Taking, as before, the continuous limit of their Eq. (37), with $q = 4$ $p = 1$ and $U_{\text{crit}} = 6t\sqrt{6}$, one finds the following differential equation

$$\frac{1}{6} \frac{\partial^2 Z(z)}{\partial z^2} + 2 Z(z) (1 - u) - c Z(z)^2 = 0. \quad (\text{A27})$$

The numerical constant is estimated to be $c = 11/9^{44}$. The limiting behavior for $u \rightarrow 1$ is the solution of

$$\frac{1}{6} \frac{\partial^2 Z(z)}{\partial z^2} = c Z(z)^2,$$

namely

$$z^2 Z(z) = \frac{1}{c} = \frac{9}{11} \simeq 0.82. \quad (\text{A28})$$

Let's consider instead our Eq. (A2) that, divided by $2\epsilon_{kin} = -U_{\text{crit}}/4$, can be written as

$$0 = \frac{1}{6} \frac{\partial^2 R(z)}{\partial z^2} + R(z) - u \frac{R(z)}{\sqrt{1-R(z)^2}} \simeq \frac{1}{6} \frac{\partial^2 R(z)}{\partial z^2} + (1-u) R(z) - \frac{1}{2} R(z)^3. \quad (\text{A29})$$

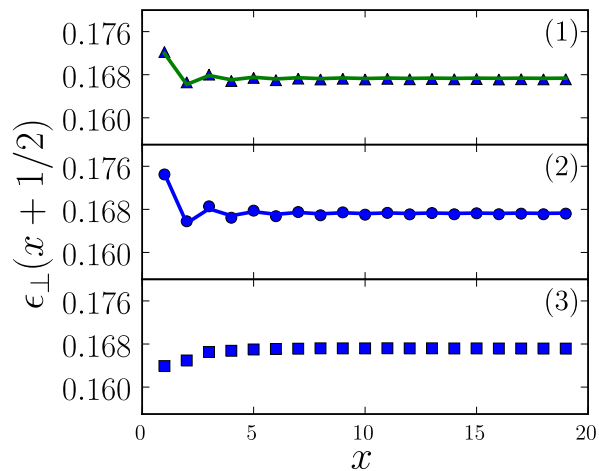


Figure 18: (Color online) Mean value of the hopping matrix element on the uncorrelated wavefunction versus the distance from the leftmost surface layer in geometry (a) with $U_{\text{surface}} = 20t$ and $U_{\text{bulk}} = 14.6642t$ (triangles, panel 1) and $U_{\text{bulk}} = 15.9712t$ (squares, panel 3). The circles in panel 2 show the hopping for the same simulation that was performed for panel 1, but as a function of distance from the right surface of the sample, where $U = U_{\text{bulk}} = 14.6642t$. The results of fit are showed by the solid lines. From above, the first and second curves are a plot of Eq. (B2) with $A = 0.1673$, $w = -0.0046$ and $A = 0.1673$, $w = -0.0074$ respectively.

At criticality, $u \rightarrow 1$, the solution

$$z^2 R(z)^2 = z^2 Z(z) = \frac{2}{3} \simeq 0.66, \quad (\text{A30})$$

is just the limiting value of Eqs. (A17) and (A11) for $\zeta = 0$. The numerical coefficient $2/3$ that we find is slightly smaller than the linearized DMFT one, $9/11$, but both are much bigger than the value extracted by straight DMFT calculations in Ref. 34, namely 0.008 . Supposedly, straight DMFT is a better approximation than linearized DMFT, which in turns should be better than our Gutzwiller technique, therefore it is likely that our results overestimate the quasiparticle residue Z .

Appendix B: FRIEDEL'S OSCILLATIONS

In the previous sections we have derived a simple model to extract the behavior of $Z(z)$ assuming uniform values for the hopping matrix elements on the uncorrelated Slater determinant. Of course the hopping is not uniform, its variation being described in most cases by some Friedel oscillations around the bulk value (thin solid lines in Figs. 2-10). The Friedel's oscillations arise as a consequence of broken translational symmetry in a Fermi gas, i.e. around a single impurity or near an interface. An

impurity embedded in an electron gas of dimensionality D induces oscillations that decay as a power law $1/r^D$ and whose wavevector is twice the Fermi wavevector⁴⁵. The Friedel's oscillations in a $D = 3$ electron gas with an interface can be obtained as a superposition of Friedel oscillations for a layer of impurities, and one can readily find that, moving perpendicularly to the interface over a length x , they behave at leading order as

$$\frac{\cos 2k_{\text{F}}x}{(2k_{\text{F}}x)^2}, \quad (\text{B1})$$

results which is strictly valid for a spherical Fermi surface, although the decay exponent is independent of the shape of the Fermi surface.

If we include electron-electron interaction via the Hubbard U and treat it by the Gutzwiller approximation, we expect that the Friedel's oscillation will be affected also by the layer-dependence of the quasiparticle weight $Z(z)$. Our results show that the faster the change of $Z(z)$, the larger the oscillations. This means that a system with geometry (a) and $U_{\text{bulk}} \lesssim U_{\text{crit}}$ displays much smoother oscillations than a system with $U_{\text{bulk}} \ll U_{\text{crit}}$, since the spatial dependence of $Z(z)$ is sharper when the bulk interaction parameter is far from criticality.

In light of the spatial dependence of the oscillations predicted by Eq. (B1), we fitted our data for the hopping $\epsilon_{\perp}(x + 1/2)$ perpendicular to the interface and in geometries (a) and (b) (see Fig. 1) with the function

$$A + w \frac{\cos \pi x}{x^2}, \quad (\text{B2})$$

where x is the distance from either the surface layer (geometry (a)) or the layer across which $U(z)$ changes stepwise (geometry (b)). The function (B2) fits the data showed in Figs. 18 for a weakly correlated system with strongly correlated surface. If the bulk value of U is increased towards U_{crit} , the correlation length ξ becomes so big that it is hard to identify unambiguously any Friedel's oscillation, as shown in Fig. 18 panel (3). The function (B2) fits also the data for the hopping on the weakly correlated side of the junction in geometry (b), see Fig. 19). On the strongly correlated (right) side of the same junction again the correlation length ξ is too large and we were not able to make any fit.

In conclusion, the inhomogeneity of the interaction parameter U affects the spatial dependence not only of the quasiparticle weight, but also of the hopping matrix element on the uncorrelated Slater determinant. The latter displays Friedel's oscillations that rise from the breaking of discrete translational symmetry. In any case, when the system is in the close vicinity of the Mott transition, the effects of these oscillations are smoothed out as a result of the diverging characteristic length ξ of the local quasiparticle weight.

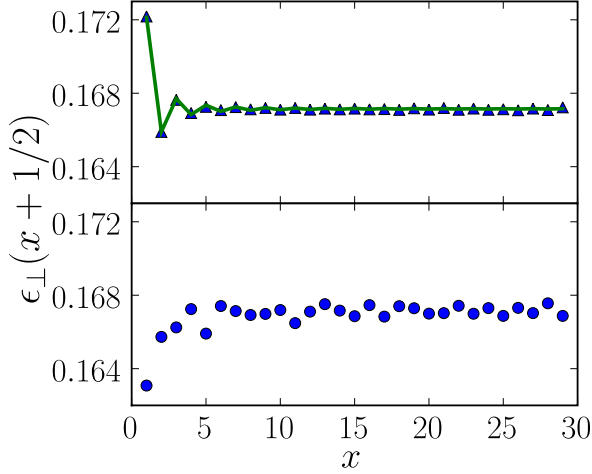


Figure 19: (Color online) Plot of the hopping matrix element for a system with geometry (b), $U_{\text{left}} = 2t$ and $U_{\text{right}} = 15.97118t$. Upper panel: x is the distance from the junction on the weakly correlated metallic (left) side; lower panel: the same on the strongly correlated metallic (right) side. The Friedel oscillations on the weakly correlated side are fitted by Eq. (B2) with $A = 0.16715$, $w = 0.0050$. On the strongly correlated side the fit was not possible for the reasons explained in the text.

-
- ¹ N. Mott, *Metal Insulator Transition* (Taylor and Francis, London, 1990).
- ² A. Georges, G. Kotliar, W. Krauth, and M. J. Rozenberg, *Rev. Mod. Phys.* **68**, 13 (1996).
- ³ A. Sekiyama, T. Iwasaki, K. Matsuda, Y. Saitoh, Y. Onuki, and S. Suga, *Nature* **403**, 396 (2000).
- ⁴ K. Maiti, D. D. Sarma, M. J. Rozenberg, I. H. Inoue, H. Makino, O. Goto, M. Pedio, and R. Cimino, *Europhys. Lett.* **55**, 246 (2001).
- ⁵ S.-K. Mo, H.-D. Kim, J. W. Allen, G.-H. Gweon, J. D. Denlinger, J.-H. Park, A. Sekiyama, A. Yamasaki, S. Suga, P. Metcalf, et al., *Phys. Rev. Lett.* **93**, 076404 (2004).
- ⁶ A. Sekiyama, H. Fujiwara, S. Imada, S. Suga, H. Eisaki, S. I. Uchida, K. Takegahara, H. Harima, Y. Saitoh, I. A. Nekrasov, et al., *Phys. Rev. Lett.* **93**, 156402 (2004).
- ⁷ N. Kamakura, Y. Takata, T. Tokushima, Y. Harada, A. Chainani, K. Kobayashi, and S. Shin, *Europhys. Lett.* **67**, 240 (2004).
- ⁸ H.-D. Kim, H.-J. Noh, K. H. Kim, and S.-J. Oh, *Phys. Rev. Lett.* **93**, 126404 (2004).
- ⁹ M. Taguchi, A. Chainani, N. Kamakura, K. Horiba, Y. Takata, M. Yabashi, K. Tamasaku, Y. Nishino, D. Miwa, T. Ishikawa, et al., *Phys. Rev. B* **71**, 155102 (2005).
- ¹⁰ S.-K. Mo, H.-D. Kim, J. D. Denlinger, J. W. Allen, J.-H. Park, A. Sekiyama, A. Yamasaki, S. Suga, Y. Saitoh, T. Muro, et al., *Phys. Rev. B* **74**, 165101 (2006).
- ¹¹ R. Eguchi, T. Kiss, S. Tsuda, T. Shimojima, T. Mizokami, T. Yokoya, A. Chainani, S. Shin, I. H. Inoue, T. Togashi, et al., *Physical Review Letters* **96**, 076402 (2006).
- ¹² M. Yano, A. Sekiyama, H. Fujiwara, Y. Amano, S. Imada, T. Muro, M. Yabashi, K. Tamasaku, A. Higashiya, T. Ishikawa, et al., *Phys. Rev. B* **77**, 035118 (2008).
- ¹³ D. B. McWhan and J. P. Remeika, *Phys. Rev. B* **2**, 3734 (1970).
- ¹⁴ D. B. McWhan, T. M. Rice, and J. P. Remeika, *Phys. Rev. Lett.* **23**, 1384 (1969).
- ¹⁵ W. F. Brinkman and T. M. Rice, *Phys. Rev. B* **2**, 4302 (1970).
- ¹⁶ P. D. Dernier and M. Marezio, *Phys. Rev. B* **2**, 3771 (1970).
- ¹⁷ G. A. Sawatzky and D. Post, *Phys. Rev. B* **20**, 1546 (1979).
- ¹⁸ K. E. Smith and V. E. Henrich, *Phys. Rev. B* **50**, 1382 (1994).
- ¹⁹ S. Shin, Y. Tezuka, T. Kinoshita, T. Ishii, T. Kashiwakura, M. Takahashi, and Y. Suda, *J. Phys. Soc. Jpn.* **64**, 1230 (1995).
- ²⁰ R. Zimmermann, R. Claessen, F. Reinert, P. Steiner, and S. Hüfner, *J. Phys.: Condens. Matter* **10**, 5697 (1998).
- ²¹ G. Panaccione, M. Altarelli, A. Fondacaro, A. Georges, S. Huotari, P. Lacovig, A. Lichtenstein, P. Metcalf, G. Monaco, F. Offi, et al., *Phys. Rev. Lett.* **97**, 116401 (2006).
- ²² S.-K. Mo, J. D. Denlinger, H.-D. Kim, J.-H. Park, J. W. Allen, A. Sekiyama, A. Yamasaki, K. Kadono, S. Suga, Y. Saitoh, et al., *Phys. Rev. Lett.* **90**, 186403 (2003).
- ²³ A. Othomo and H. Y. Hwang, *Nature* **427**, 423 (2004).
- ²⁴ N. Reyren, S. Thiel, A. D. Caviglia, L. F. Kourkoutis, G. Hammerl, C. Richter, C. W. Schneider, T. Kopp, A.-S. Ruetschi, D. Jaccard, et al., *Science* **317**, 1196 (2007).
- ²⁵ See e.g. Refs. 46,47,48 and MRS Bulletin, volume **33**

- (2008), for an overview of the status and perspectives of this subject.
- ²⁶ R. Pentcheva and W. E. Pickett, Phys. Rev. B **74**, 035112 (2006).
- ²⁷ S. Schwieger, M. Potthoff, and W. Nolting, Phys. Rev. B **67**, 165408 (2003).
- ²⁸ M. Potthoff and W. Nolting, Phys. Rev. B **60**, 7834 (1999).
- ²⁹ S. Okamoto and A. J. Millis, Nature **428**, 630 (2004).
- ³⁰ S. Okamoto and A. J. Millis, Phys. Rev. B **70**, 241104 (2004).
- ³¹ J. Freericks, Phys. Rev. B **70**, 195342 (2004).
- ³² A. Liebsch, Phys. Rev. Lett. **90**, 096401 (2003).
- ³³ L. Chen and J. K. Freericks, Physical Review B (Condensed Matter and Materials Physics) **75**, 125114 (pages 8) (2007).
- ³⁴ R. W. Helmes, T. A. Costi, and A. Rosch, Phys. Rev. Lett. **101**, 066802 (2008).
- ³⁵ H. Zenia, J. K. Freericks, H. R. Krishnamurthy, and T. Pruschke, Physical Review Letters **103**, 116402 (pages 4) (2009).
- ³⁶ H. Ishida, D. Wortmann, and A. Liebsch, Phys. Rev. B **73**, 245421 (2006).
- ³⁷ F. Rodolakis, B. Mansart, E. Papalazarou, S. Gorovikov, P. Vilmercati, L. Petaccia, A. Goldoni, J. P. Rueff, S. Lupi, P. Metcalf, et al., Phys. Rev. Lett. **102**, 066805 (2009).
- ³⁸ G. Borghi, M. Fabrizio, and E. Tosatti, Phys. Rev. Lett. **102**, 066806 (2009).
- ³⁹ M. C. Gutzwiller, Phys. Rev. **134**, A923 (1964).
- ⁴⁰ M. C. Gutzwiller, Phys. Rev. **137**, A1726 (1965).
- ⁴¹ M. Fabrizio, Phys. Rev. B **76**, 165110 (2007).
- ⁴² J. Bünemann, F. Gebhard, T. Ohm, S. Weiser, and W. Weber, in *Frontiers in Magnetic Materials*, edited by A. Narlikar (Springer, Berlin, 2005), pp. 117–151.
- ⁴³ H. J. Monkhorst and J. D. Pack, Phys. Rev. B **13**, 5188 (1976).
- ⁴⁴ R. Bulla and M. Potthoff, Eur. Phys. J. B **13**, 257 (2000).
- ⁴⁵ G. Giuliani and G. Vignale, *Quantum Theory of the Electron Liquid* (Cambridge University Press, 2005).
- ⁴⁶ J. Heber, Nature **459**, 28 (2009).
- ⁴⁷ B. Goss Levi, Physics Today **60**, 23 (2007).
- ⁴⁸ J. W. Reiner, F. J. Walker, and C. H. Ahn, Science **323**, 1018 (2009).